Clinical Cancer Research

Radiation Enhancement of Head and Neck Squamous Cell Carcinoma by the Dual PI3K/mTOR Inhibitor PF-05212384

Andrew J. Leiker[1,2], William DeGraff[1], Rajani Choudhuri[1], Anastasia L. Sowers[1], Angela Thetford[1], John A. Cook[1], Carter Van Waes[3], and James B. Mitchell[1]

Abstract

Purpose: Radiation remains a mainstay for the treatment of nonmetastatic head and neck squamous cell carcinoma (HNSCC), a malignancy characterized by a high rate of PI3K/mTOR signaling axis activation. We investigated the ATP-competitive dual PI3K/mTOR inhibitor, PF-05212384, as a radiosensitizer in preclinical HNSCC models.

Experimental Design: Extent of radiation enhancement of two HNSCC cell lines (UMSCC1-wtP53 and UMSCC46-mtP53) and normal human fibroblast (1522) was assessed by *in vitro* clonogenic assay with appropriate target inhibition verified by immunoblotting. Radiation-induced DNA damage repair was evaluated by γH2AX Western blots with the mechanism of DNA double-strand break repair abrogation investigated by cell cycle analysis, immunoblotting, and RT-PCR. PF-05212384 efficacy *in vivo* was assessed by UMSCC1 xenograft tumor regrowth delay, xenograft lysate immunoblotting, and tissue section immunohistochemistry.

Results: PF-05212384 effectively inhibited PI3K and mTOR, resulting in significant radiosensitization of exponentially growing and plateau-phase cells with 24-hour treatment following irradiation, and variable radiation enhancement with 24-hour treatment before irradiation. Tumor cells radiosensitized to a greater extent than normal human fibroblasts. Postirradiation PF-05212384 treatment delays γH2AX foci resolution. PF-05212384 24-hour exposure resulted in an evident G_1–S phase block in p53-competent cells. Fractionated radiation plus i.v. PF-05212384 synergistically delayed nude mice bearing UMSCC1 xenograft regrowth, with potential drug efficacy biomarkers identified, including pS6, pAkt, p4EBP1, and Ki67.

Conclusions: Taken together, our results of significant radiosensitization both *in vitro* and *in vivo* validate the PI3K/mTOR axis as a radiation modification target and PF-05212384 as a potential clinical radiation modifier of nonmetastatic HNSCC. *Clin Cancer Res; 21(12); 2792–801. ©2015 AACR.*

Introduction

Despite significant advances in the treatment of nonmetastatic head and neck squamous cell carcinoma (HNSCC), the 5-year disease-specific survival rate remained poor at approximately 66% from 2002 to 2006 (1, 2). Although improved from approximately 55% a decade earlier, increased survival arose partially secondary to an epidemiologic shift [↑HPV (human papillomavirus) rate]; thus, the necessity to improve HPV-negative HNSCC treatment remains critical as ever. In an attempt to improve outcomes, research efforts have subsequently shifted to focus on rational-based treatments via molecularly targeting oncogenic signaling pathways. In two landmark phase III clinical trials, the molecularly targeted EGFR inhibitor cetuximab, a chimeric monoclonal antibody, in combination with radiation or platinum-fluorouracil for the treatment of HNSCC demonstrated an absolute survival benefit of 10% and 20%, respectively (3, 4). Although improving overall survival, given the near ubiquitous overexpression (≥90%) of EGFR in HNSCC, the demonstrated benefit of cetuximab was lower than anticipated (5). The two aforementioned trials did, however, demonstrate the validity of molecularly targeted therapy for the treatment of HNSCC. Excluding early disease, radiation alone or in combination with other modalities plays a central role in the treatment of all anatomical sites of HNSCC (6). The pivotal role radiation plays in the treatment of HNSCC warrants preclinical investigation into identifying better novel molecularly targeted radiation modifiers.

The Cancer Genome Atlas (TCGA) and other studies have rapidly identified numerous cancer cell–dysregulated signaling pathways (7–9). Among the identified HNSCC aberrations, the most prevalent of genetic and epigenetic alterations lie along the PI3K/Akt/mTOR pathway. The PI3K/Akt/mTOR axis is a central signaling pathway that plays a crucial role in metabolism, cell growth, apoptosis, survival, and differentiation (10). Genetic aberrations along this key axis can lead to persistent activation and consequently a malignant phenotype. Along with driving malignancy, the PI3K/Akt/mTOR signaling cascade has been implicated in the radiation response and radioresistance (11–14).

Molecularly targeted agents inhibiting PI3K and mTOR have been tested in preclinical models, and as expected demonstrated significant radiation enhancement (15–17). An orally available dual PI3K/mTOR inhibitor, PF-04691502, in preliminary studies

[1]Radiation Biology Branch, Center for Cancer Research, National Cancer Institute, NIH, Bethesda, Maryland. [2]Medical Research Scholars Program, NIH, Bethesda, Maryland. [3]Head and Neck Surgery Branch, NIDCD, NIH, Bethesda, Maryland.

Note: Supplementary data for this article are available at Clinical Cancer Research Online (http://clincancerres.aacrjournals.org/).

Corresponding Author: James B. Mitchell, NCI, NIH, Bldg. 10, Room B3-B69, 9000 Rockville Pike, Bethesda, MD 20892. Phone: 301-402-9013; Fax: 301-480-2238; E-mail: jbm@helix.nih.gov

doi: 10.1158/1078-0432.CCR-14-3279

Translational Relevance

Combined modality treatment of locoregional head and neck squamous cell carcinoma (HNSCC) has improved outcomes over the last two decades, but 5-year survival rates remain poor with significant morbidity. Thus, there is an urgent necessity to improve treatment outcomes without added toxicity. This study reports the evaluation of PF-05212384, a novel dual PI3K/mTOR inhibitor currently in phase I to II clinical trials, as an HNSCC radiation sensitizer. Selectively targeting the PI3K/mTOR axis significantly radiosensitized proliferative tumor cell lines, plateau-phase tumor cells, and tumor xenografts, with only minimal normal fibroblast radiosensitization. These data suggest the PI3K/mTOR axis is a potential selective radiation target for malignant head and neck squamous cells and warrants assessment of PF-05212384 in clinical trials as a radiation modifier.

has demonstrated HNSCC radiosensitization with single fraction radiation *in vivo* (17). In addition, a dual PI3K/mTOR inhibitor, NVP-BEZ-235, has displayed radiosensitization in numerous preclinical studies (18–20). However, Mukherjee and colleagues have eloquently demonstrated that the radiosensitizing effect propagated by NVP-BEZ-235 is in part secondary to catalytic inhibition of the ATM and DNA-PKc enzymes (21, 22). The ATM and DNA-PKc protein kinases are critical components of the DNA-DSB (double-strand break) repair response and belong to the PI3K-like kinase (PIKK) family, along with PI3K, mTORC1, and mTORC2 (23, 24). DNA repair enzyme inhibition radiosensitization may be a viable approach in select anatomic sites, but normal tissue radiosensitization will likely limit this approach clinically for the vast majority of malignancies (25). Unlike quiescent normal tissue sites, a majority of the aerodigestive tract irradiated during the course of HNSCC treatment comprises rapidly dividing mucosal epithelium, adding credence to identifying selective radiation modifiers. The necessity to selectively target HNSCC versus normal tissue is reinforced by RTOG 0522, a randomized phase III clinical trial of radiation and cisplatin with or without cetuximab for locally advanced HNSCC. Disappointingly, survival was not improved when adding cetuximab, which may have been a consequence of radiotherapy interruptions (~27%) secondary to added toxicity (26).

We hypothesize that given PI3K/Akt/mTOR pathway's oncogenic role in HNSCC, along with early PF-04691502 single radiation fraction data, that dual PI3K/mTOR inhibition by PF-05212384, an intravenous delivered compound currently in phase I to II clinical trials, would result in significant HNSCC radiosensitization, and to a greater extent than normal tissue (17, 27). To test this hypothesis, we performed clonogenic survival studies in HNSCC cell lines, including nondividing cells (G_1 enriched) and normal tissue. To identify the most appropriate clinical regimen, separate *in vitro* drug regimens before and after irradiation were studied. With significant radiation enhancement identified, we went on to validate appropriate target inhibition by *in vitro* Western blotting, as well as identify potential radiation enhancement mechanism by cell cycle analyses, DNA-DSB repair assay, and senescence pathway–directed RT-PCR genomic expression analysis. In addition, the ability of PF-05212384 to radiosensitize *in vivo* in combination with fractionated radiation was tested in a human HNSCC xenograft model. Associated xenograft harvests were additionally utilized to assess *in vivo* target inhibition as well as potentially identify clinical biomarkers.

Materials and Methods

Cell culture and drug solutions

UMSCC1 wild-type p53 (HNSCC) and UMSCC46 mutant-type p53 (HNSCC) were kindly provided by Dr. Thomas E. Carey (University of Michigan, Ann Arbor, MI) and were grown in MEM supplemented with 10% FBS and streptomycin/penicillin (17). FaDu (mutant-type p53) was purchased from the American Type Culture Collection (ATCC) and maintained in DMEM supplemented with 10% FBS and streptomycin/penicillin (28). Normal human lung fibroblasts (1522) were purchased from the Coriell Institute for Medical Research and were grown in Nutrient Mixture F12 supplemented with 20% FBS and streptomycin/penicillin. Cell culture maintenance and all *in vitro* work were performed at atmospheric oxygen levels (21% O_2; 5% CO_2). All cell lines were authenticated within the past 6 months by IDEXX Bioresearch using Cell Check 9 [9 allele marker STR (short tandem repeat) profile and interspecies contamination test]. For *in vitro* studies, PF-05212384 (Pfizer and Selleck Chemicals) was dissolved in dimethyl sulfoxide and stored in aliquots of 10 mmol/L concentration at −70°C. For xenograft tumor growth delay, PF-05212384 was dissolved in 5% dextrose/0.25% lactic acid at 1 mg/mL and raised to a pH of 3.3 with 1 mol/L NaOH.

Cell survival studies

Cells were plated (5×10^5) in 100-mm dishes and incubated overnight at 37°C. Exponentially growing cells were subsequently exposed to 10 μmol/L PF-05212384 for 24 hour, then irradiated (PF-05212384 removed immediately following ionizing radiation, IR), or irradiated and immediately exposed to 10 μmol/L PF-05212384 for 24 hours in separate experiments. For plateau-phase clonogenic survival, UMSCC1 cells were grown to confluence with G_1 phase enrichment verification by cell cycle analysis; confluent cells were then subsequently treated as described above. Following drug exposure and irradiation, cells were rinsed, trypsinized, counted, and plated in triplicate for macroscopic colony formation and allowed to grow for 10 to 14 days at 37°C. Colonies were fixed and stained with methanol/crystal violet, and counted. After correcting for plating efficiency and PF-05212384 toxicity, survival data were plotted and fitted with the linear quadratic model according to Albright (29). The dose modification factor (DMF) for each clonogenic survival curve was calculated as the control (DMSO) radiation dose for 10% survival divided by radiation dose for 10% survival with PF-05212384 treatment (30). DMFs are subsequently expressed as the mean and SEM of multiple experiments.

Immunoblotting

For 24-hour PF-05212384 exposure then irradiation, exponentially growing cells were washed twice with 37°C fresh medium immediately following irradiation and collected as a function of time following irradiation. Total protein from cultured cells, excluding γH2AX, and xenograft tumor protein extraction was performed as previously described (30). Acid soluble histone proteins were extracted in 0.2 mol/L sulfuric acid as previously described (31). Protein concentrations were determined with a DC-Protein Assay (Bio-Rad); samples were then aliquoted and stored at −70°C. Protein samples of equal amount (5–40 μg) were

subjected to SDS PAGE on 4% to 20% Novex Tris-Glycine gels or NuPAGE 3% to 8% Tris-Acetate gels (Invitrogen). Proteins were then transferred to a nitrocellulose membrane using an iBlot Dry Blotting System (Invitrogen). Nitrocellulose membranes were then incubated with primary antibody according to manufacturer-recommended dilutions overnight with gentle agitation at 4°C followed by incubation with the appropriate secondary antibody (1:2,000) for 1 hour at room temperature. Protein bands were visualized by chemiluminescence (Thermo Scientific). To ascertain equal protein loading and transfer, antibody was stripped by ReBlot Plus mild antibody stripping solution (Millipore), and membranes were probed with the appropriate loading control. Protein band image capture and quantification were performed with a Fluor Chem HD2 imager (Alpha Innotech) coupled with image analyzer software. Density values for each band were normalized to the appropriate loading control and expressed as fold change compared with control condition. The following primary antibodies were used: pS6 (Cell Signaling Technology; #5364), S6 (Cell Signaling Technology; #2217), p4EBP1 (Cell Signaling Technology; #2855), 4EBP1 (Cell Signaling Technology; #9644), pAkt (Cell Signaling Technology; #9271), Akt (Cell Signaling Technology; #9272), pH2AX (Upstate; #05636), H2A (Millipore; #07146), pATM (Cell Signaling Technology; #5883), ATM (Cell Signaling Technology; #2873), pDNA-PKc (Cell Signaling Technology; #4215), DNA-PKc (Cell Signaling Technology; #4602), p21 (BD Pharmingen; #554228), p27 (Epitomics; #27471), p53 (Abcam; ab32049), Actin (Millipore; MAB1501R), Cyt C (Santa Cruz; G2909), HSC70 (Santa Cruz; J2212).

Xenograft studies

All animal experiments were carried out in accordance with protocols approved by the National Cancer Institute's Animal Care and Use Committee (ACUC). For radiation regrowth delay studies, UMSCC1 cells (1.0×10^6) were injected into the subcutaneous space of the right hind leg of athymic nude mice, 5 to 6 weeks of age, bred at the National Cancer Institute's Animal Production Area (Frederick, MD). Individual mice were ear tagged and randomized on day 6 of tumor growth into the following 4 groups (8 mice/group): vehicle control, vehicle control + fractionated radiation, PF-05212384 control, and PF-05212384 + fractionated radiation. Fractionated radiation (3 Gy) was delivered daily for two full work weeks starting on Monday with a hiatus of two days following five fractions, with a total dose of 30 Gy delivered. PF-05212384 (6.7 mg/kg) was delivered via tail vein injection (<200 μL) 2 hours before Monday, Wednesday, and Friday's fractionated radiation with an additive total of 40 mg/kg. Two to three additional mice per group were treated in parallel for tumor harvest. UMSCC1 tumor xenografts were harvested 2 hours following the third PF-05212384 injection and fifth 3-Gy fractionated radiation dose. Tumor samples were immediately divided with one piece flash frozen in liquid nitrogen for immunoblotting and the second embedded with Tissue-Tek OCT (optimal cutting temperature) compound (Sakura Finetek USA) over dry ice followed by storage at 70°C. Individual mice tumor volume growth data were fitted with an exponential growth curve, and days to thrice starting tumor volume were determined. For control and treated groups, growth delay is expressed as mean time (days) to thrice starting tumor volume.

Cell cycle analysis, RT-PCR, immunohistochemistry, and irradiation

Cell cycle analysis, RT-PCR genomic expression analysis, immunohistochemistry, and irradiation technique followed standard experimental methodology (32, 33). A detailed breakdown can be found in Supplementary Materials and Methods.

Statistical analyses

Statistically significant differences for immunofluorescence densitometry, immunohistochemistry total fluorescence, and xenograft group growth differences were assessed using the Student *t* test in Microsoft Excel.

Results

PF-05212384 sensitizes HNSCC to radiation

To determine the ability of PF-05212384 to radiosensitize HNSCC, pilot studies were performed indicating radiation enhancement both with preirradiation PF-05212384 (10 μmol/L) treatment and postirradiation PF-05212384 (10 μmol/L) treatment protocols. Radiation enhancement was optimized with 24-hour drug exposure regardless of pre- or postirradiation treatment protocols (Supplementary Fig. S1A). Minimal toxicity was observed for the majority of cell lines treated with PF-05212384 alone (Table 1). Treatment with PF-05212384 24 hours before irradiation led to enhancement in radiosensitivity in UMSCC1 cells, with a DMF (±SEM) of 1.9 ± 0.07. UMSCC46 cancer cells and normal human fibroblasts (1522) displayed no pretreatment radiation enhancement (Fig. 1A–C). Post-IR PF-05212384 treatment radiation enhancement was observed in all cell lines studied, with PF-05212384 enhancing radiation to a greater extent in HNSCC cells than normal human fibroblasts (DMFs, UMSCC1—3.6 and UMSCC46—1.9 vs. 1522—1.4, Fig. 1D–F). A third HNSCC line (FaDu) was exquisitely sensitive to PF-05212384 treatment alone, and displayed both pre- and post-IR PF-05212384 treatment radiation enhancement (Supplementary Fig. S1D). All data described to this point apply to exponentially growing cells. Radiation enhancement, although reduced, was observed with both 24-hour pre-IR and 24-hour post-IR PF-05212384

Table 1. Summary of DMFs, PF-05212384 (10 μmol/L) toxicity alone, and PF-05212384 impact on cell cycle distribution

	24-hour pre-XRT treat DMF (±SEM)	24-hour post-XRT treat DMF (±SEM)	24-hour PF-384 (10 μmol/L) exposure (no IR)			
			Surviving fraction (±SEM)	G_1(%)[a] (Control G_1%)	S(%) (Control S%)	G_2–M(%) (Control G_2–M%)
UMSCC1	1.9 (±0.07)	3.6 (±0.14)	0.71 (±0.06)	88% (39%)	6% (56%)	6% (5%)
UMSCC46	1.0 (±0.00)	1.9 (±0.25)	0.84 (±0.09)	45% (32%)	24% (43%)	31% (25%)
1522	1.0 (±0.00)	1.4 (±0.15)	0.84 (±0.06)	81% (65%)	3% (21%)	17% (15%)
UMSCC1 (plateau)	1.6 (±0.05)	2.2 (±0.55)	0.62 (±0.03)	87% (69%)	7% (26%)	6% (5%)

[a]Cell cycle distribution plots are shown in Supplementary Fig. S2. Cell cycle distribution data representative of multiple experiments.

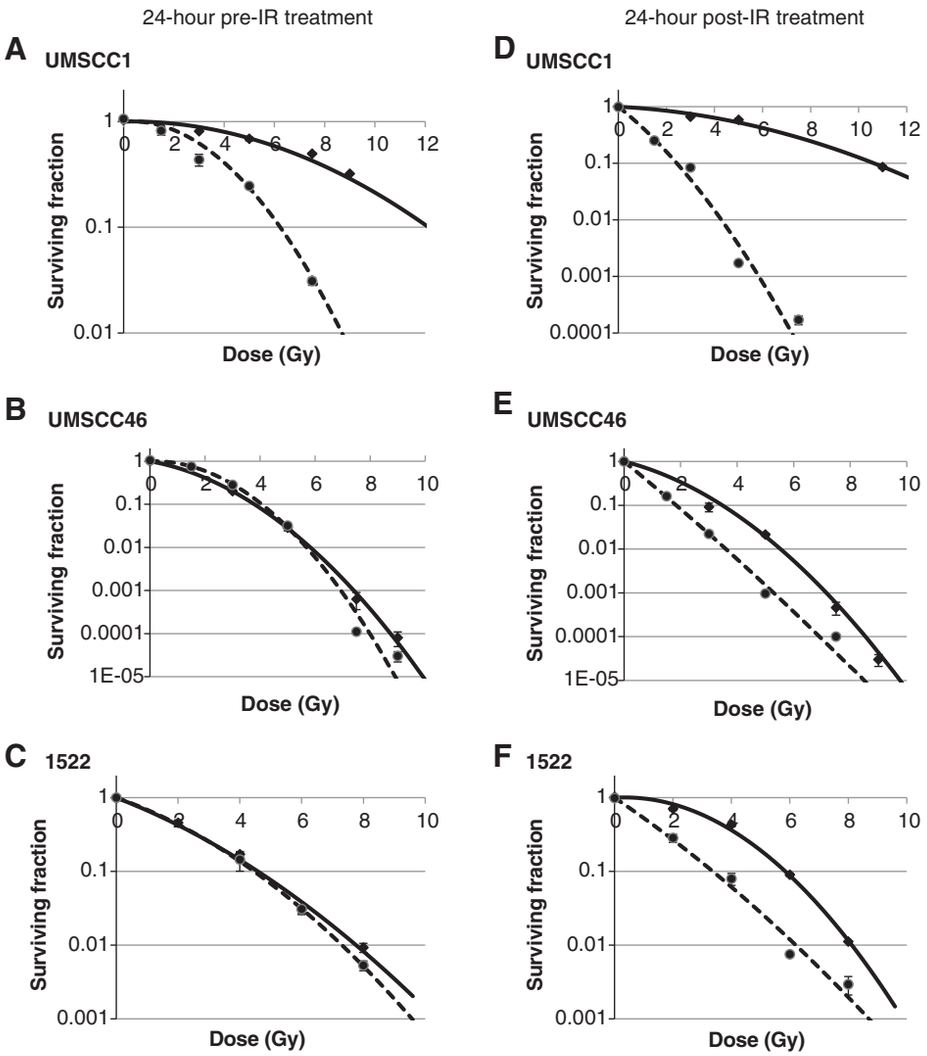

Figure 1.
Radiation survival curves for cell lines treated with PF-05212384 (10 μmol/L, dashed curve) or with DMSO control (0.1%, solid curve) for 24 hours before irradiation [pre-IR treatment, (A–C) UMSCC1, UMSCC46, and 1522], or for 24 hours following irradiation [post-IR treatment, (D–F) UMSCC1, UMSCC46, and 1522]. Data representative of 2 to 3 independent experiments fitted using the linear quadratic model. DMFs and drug treatment toxicities are shown in Table 1.

treatment (DMFs of 1.6 and 2.2, respectively) of plateau-phase UMSCC1 cells (Table 1; Supplementary Fig. S1B and S1C). UMSCC1 confluence (plateau phase) was verified with G_1 phase enrichment of approximately 70% in confluent cells versus approximately 40% in exponentially growing cells (Table 1). Reduced radiation enhancement in plateau-phase cells indicates some dependence on active cell cycling.

PF-05212384 in the setting of radiation prolongs PI3K/mTOR signaling cascade knockdown

To identify possible variable drug response contributing to differential radiation enhancement, we next investigated the downstream targets of the PI3K/mTOR cascade (phosphorylated-S6, phosphorylated-4EBP1, and phosphorylated-Akt) with both pre-IR PF-05212384 treatment and post-IR PF-05212384 treatment. Reduced inhibition of 4EBP1 phosphorylation (not pS6 alone) secondary to mTORC1 inhibitor resistance has previously been shown to correlate with limited radiation enhancement and drug response (34, 35). UMSCC1 and UMSCC46 cells were treated with PF-05212384 (10 μmol/L) for 24 hours then irradiation with immunoblots demonstrating a dramatic reduction in total p4EBP1 (with or without IR) >24 hours following irradiation; the same effect was observed with the mTORC1 target S6 (Fig. 2A and B). PF-05212384 treatment following irradiation resulted in a reduction in mTORC1 target protein phosphorylation (with or without IR) with only 2 hours of treatment (Supplementary Fig. S3A and S3B). In addition, treatment with PF-05212384 (10 μmol/L) dramatically reduced mTORC2 phosphorylation of Akt (Fig. 3C). Given the central role mTOR plays in integrating metabolic and growth signaling and its intricate interplay with the tumor suppressor p53, we assessed for cell cycle perturbation secondary to PI3K/mTOR inhibition (24-hour PF-05212384 exposure) with or without radiation (36). PF-05212384 exposure (24 hours) alone induced significant cell cycle G_1 arrest, in FaDu (72% vs. 49% control), UMSCC1 (88% vs. 39% control), and 1522 (81% vs. 65% control). The increase in G_1 was mirrored by a reduction in S-phase in these 3 cell lines. As has been seen with another dual PI3K/mTOR inhibitor, the UMSCC46 cells had a much reduced G_1 phase increase after PF-05212384 incubation (45% vs. 32% control) and little reduction in S-phase (Table 1; Supplementary Fig. S2A; ref. 17). PF-05212384 treatment following irradiation (8 Gy) did not abrogate radiation-induced G_2–M arrest (data not shown), which corresponds well to Cyclin B1 downregulation both with irradiation and drug treatment

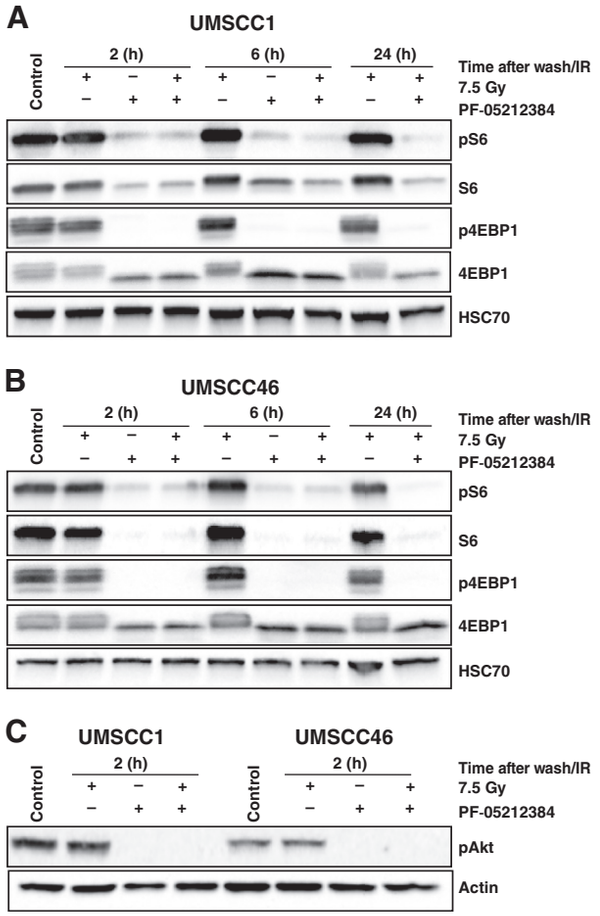

Figure 2.
The effects of PF-05212384 on the phosphorylation of the PI3K/mTOR downstream targets S6, 4EBP1, and Akt. A–C, UMSCC1 and UMSCC46 HNSCC cells were treated with PF-05212384 (10 μmol/L) for 24 hours and then irradiated (7.5 Gy); immediately following irradiation, cells were washed twice with 37°C medium and were subsequently incubated with drug-free medium for the given timeframe. PF-05212384 effect on PI3K/mTOR targets with treatment following irradiation demonstrated in Supplementary Fig. S3A and S3B.

(Supplementary Table S1). Similarly to the oral dual PI3K/mTOR inhibitor PF-04691502, dual PI3K/mTOR inhibition by PF-05212384 induced p53, p21, and p27 expression in UMSCC1 cells (Supplementary Fig. S2; ref. 17). PF-0521384 incubation did not significantly change p53, p21, or p27 in the p53-mutated UMSCC46 cells (Supplementary Fig. S2), and this corresponded to the lack of G_1 inhibition in the USMCC46 cells (Table 1).

PF-05212384 significantly inhibits radiation-induced DNA-DSB repair with post-IR treatment

We investigated the influence PF-05212384 has on radiation-induced DNA damage by assessment of phosphorylated γH2AX induction and resolution. Immunoblots demonstrating PF-05212384 impact on phosphorylated γH2AX kinetics, in UMSCC1, are shown in Fig. 3A–C for both pre-IR and post-IR treatment protocols. As expected, relative phosphorylated γH2AX rapidly increased (0.5 hours) following cell irradiation, but with resolution of radiation-induced DNA-DSBs 24 hours following radiation in nontreatment controls. With post-IR 24-hour treatment, PF-05212384 resulted in a persistent elevation of phosphorylated γH2AX significantly ($P < 0.05$) different from 24-hour radiation control (Fig. 3A and B). In addition, PF-05212384 24-hour exposure alone resulted in a significant ($P < 0.05$) reduction in total phosphorylated γH2AX versus control (Fig. 3A and B). With post-IR treatment in UMSCC46, multiple experiments indicated phosphorylated γH2AX was significantly ($P < 0.05$) elevated in PF-05212384 + radiation (4 Gy) versus radiation (4 Gy) control at 6 hours after IR (Supplementary Fig. S4). Twenty-four–hour PF-05212384 treatment followed by irradiation, although appearing to impede DNA-DSB repair, did not result in a statistically significant difference in phosphorylated γH2AX resolution versus radiation control at 24 hours after IR across multiple independent experiments (Fig. 3C). As is suggested by PF-05212384 post-IR treatment γH2AX data, radiation modulation is at least in part secondary to mitigation of key components of the DNA-DSB repair pathway. ATM and DNA-PKc protein

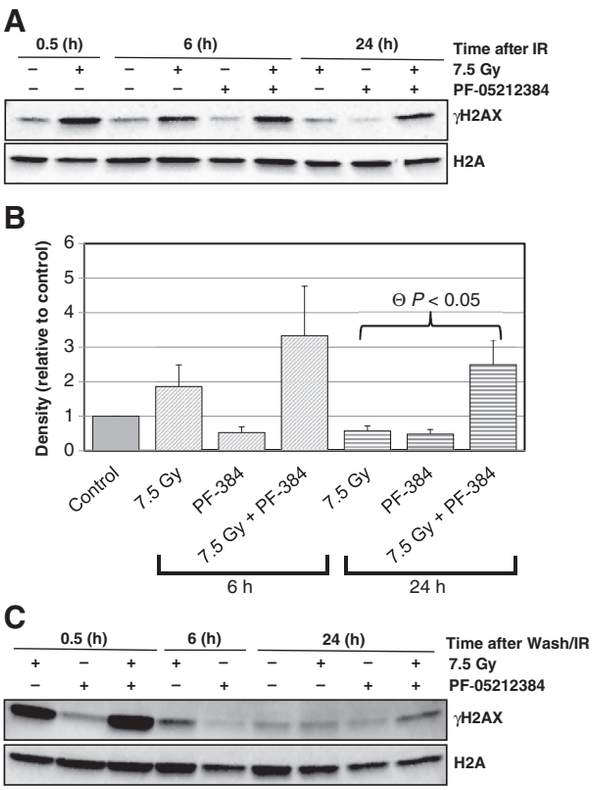

Figure 3.
The effects of PF-05212384 (10 μmol/L) on UMSCC1 radiation induced DNA damage repair. Western blot analysis of phosphorylated γH2AX from (A) UMSCC1 as a function of PF-05212384 (10 μmol/L) drug treatment time following irradiation (7.5 Gy) with associated (B) mean (±SEM) densitometry of three independent γH2AX post-IR PF-05212384 treatment westerns. Individual experiment densitometry results were normalized based on the corresponding lane H2A loading control. Characteristic Western blot of γH2AX from (C) UMSCC1 as a function of time following irradiation (7.5 Gy) with 24-hour PF-05212384 (10 μmol/L) pre-IR treatment; DNA-DSB repair inhibition at 24 hours is not statistically significant across multiple independent experiments. With pre-IR treatment, cells washed twice with 37°C medium at time of irradiation and incubated with drug-free medium for the given timeframe. Statistically significant difference indicated by ⊖ as calculated by the Student *t* test.

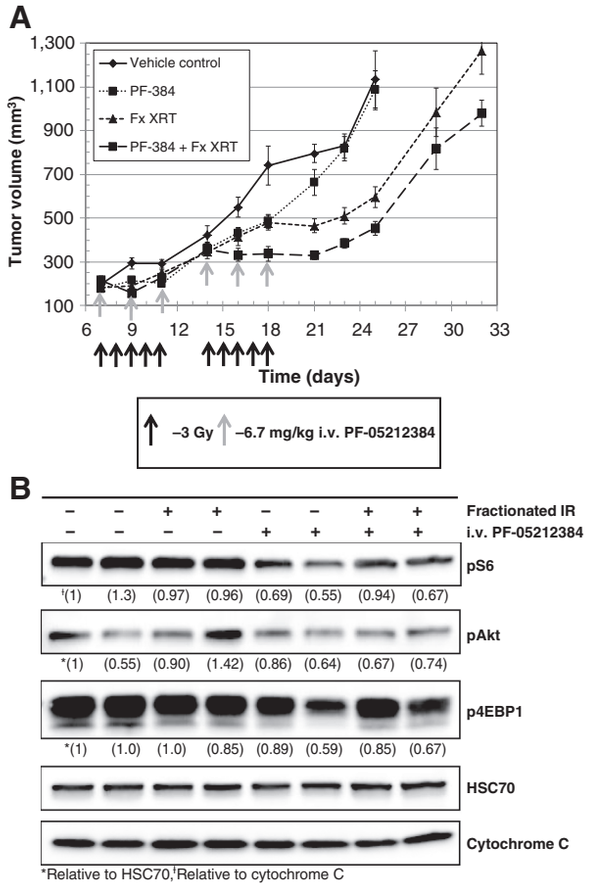

Figure 4.
Radiation modulation of UMSCC1 tumor xenografts by dual PI3K/mTOR inhibition via PF-05212384 treatment. A, athymic nude mice bearing right flank UMSCC1 tumor xenografts were treated with fractionated radiation (daily 3 Gy fraction Monday to Friday × 2 weeks) with and without i.v. PF-05212384 (6.7 mg/kg Monday, Wednesday, and Friday 2 hours before radiation fraction). Xenograft regrowth delays (±SEM) relative to the control arm for i.v. PF-05212384, fractionated radiation (30 Gy total), and i.v. PF-05212384 plus fractionated radiation were as follows: 3.1 ± 0.9 days, 7.1 ± 1.4 days, and 13.0 ± 1.6 days, respectively. Fractionated radiation plus PF-05212384 regrowth delay is significantly different from fractionated radiation alone regrowth delay ($P < 0.05$; Student t test). B, immunoblots of the PI3K/mTOR downstream targets S6, Akt, and 4EBP1 from UMSCC1 xenografts harvested 2 hours following the fifth 3 Gy fraction and third PF-05212834 injection. Each lane (column) represents one UMSCC1 xenograft harvest. Normalized protein densities for each band are in parentheses below each row.

kinases belong to the PIKK family, along with PI3K, mTORC1, and mTORC2 (21–23). Given the considerable homology between the catalytic sites of the previously listed protein kinases, we performed immunoblots investigating ATM and DNA-PKc activation following IR with and without PF-05212384 treatment. Treatment with PF-05212384 following IR did not impact resulting DNA-PKc or ATM protein kinase activation (Supplementary Fig. S5A). Treatment with PF-05212384 for 24 hours then IR followed by cellular incubation with drug-free medium for 2 hours (sample then extracted) demonstrated a slight reduction in total phosphorylated DNA-PKc, but not phosphorylated ATM, with 7.5 Gy + PF-05212384 versus 7.5 Gy alone (Supplementary Fig. S5B). However, these data when normalized to total DNA-PKc for the given sample time point demonstrate minimal to no DNA-PKc catalytic site inhibition. Our assessment of total phosphorylated ATM and DNA-PKc with PF-05212384 treatment (±IR) demonstrates DNA-DSB repair inhibition although mitigated is likely not secondary to direct ATM or DNA-PKc catalytic site inhibition.

IR plus PF-05212384 *in vitro* does not accelerate cellular senescence

The interplay between the PI3K/mTOR signaling cascade and the two central regulators of cellular senescence, p53 and Rb, is intricate and yet to be fully understood (37, 38). Given the significant association, we performed senescence pathway–directed RT-PCR genomic expression analysis investigating accelerated senescence on the order of days as a potential mechanism of PF-05212384–reduced clonogenicity and impeded repair of radiation-induced DNA-DSB following IR. Another valuable *in vitro* cellular senescence analysis, β-galactosidase staining, was considered, but provided no information as β-galactosidase staining of the HNSCC cell lines under investigation leads to cellular morphology changes, cell culture detachment, and cell death. Azad and colleagues demonstrated accelerated senescence of irradiated human cancer cells with NVP-BEZ-235 treatment, thought to be secondary to selective DNA-PKc inhibition (39). siRNA DNA-PKc knockdown provided distinct evidence of the role DNA-PKc inhibition plays in irradiated tumor cell–accelerated senescence, but without studies investigating siRNA and NVP-BEZ-235 cotreatment, dual PI3K/mTOR inhibition cannot be ruled out as a contributing factor. For our analysis, exponentially growing UMSCC1 cells were treated with 24-hour PF-05212384 (10 μmol/L) or DMSO (0.1%) followed by irradiation (10 Gy) or mock irradiation. mRNA was collected 24 hours following irradiation for analysis with a cellular senescence microarray kit. In addition, one set of UMSCC1 cells was irradiated and treated with PF-05212384 as stated above, but 24 hours following irradiation cells were washed with 37°C medium and left to recover for 48 hours; mRNA was then extracted for senescence gene analysis. All 84 genes were compared with control-untreated UMSCC1 cells with 77 giving measurable signal for unsupervised clustering analysis. The heat map for the drug and IR exposure is shown in Supplementary Fig. S6. First, immediately after IR exposure, only 3 transcripts were upregulated (>2-fold ratio) and 4 were downregulated (<0.5 ratio) compared with control-untreated cells. In contrast, the PF-05212384 24-hour–treated cells had 11 upregulated and 44 downregulated genes. The heat map clearly shows that PF-05212384 treatment dominated the gene response, and the addition of IR did little to alter this response. Forty-eight hours after PF-05212384 was washed away, many of the 77 genes were beginning to return to control levels (ratio = 1) with 2 major cell cycle/damage response genes p53 and CDKN1C going from a ratio of 15.6 to 1.2 and 9.0 to 1.4, respectively (Supplementary Table S1). Secondly, two genes measured qualitatively changed in the same manner as the proteins measured (AKT1, p21). Finally, genes involved with DNA damage response were greatly reduced by PF-05212384 exposure, and several were not recovered after wash out followed by additional 48-hour incubation. An interesting finding of the RT-PCR analysis is the significant upregulation of fibronectin 1 (>100-fold change; Supplementary Table S1). Experimental data indicate cellular adhesion to fibronectin activates PI3K (40). In addition, fibronectin 1 has been implicated as a biomarker of HNSCC radiosensitization (41). The increased

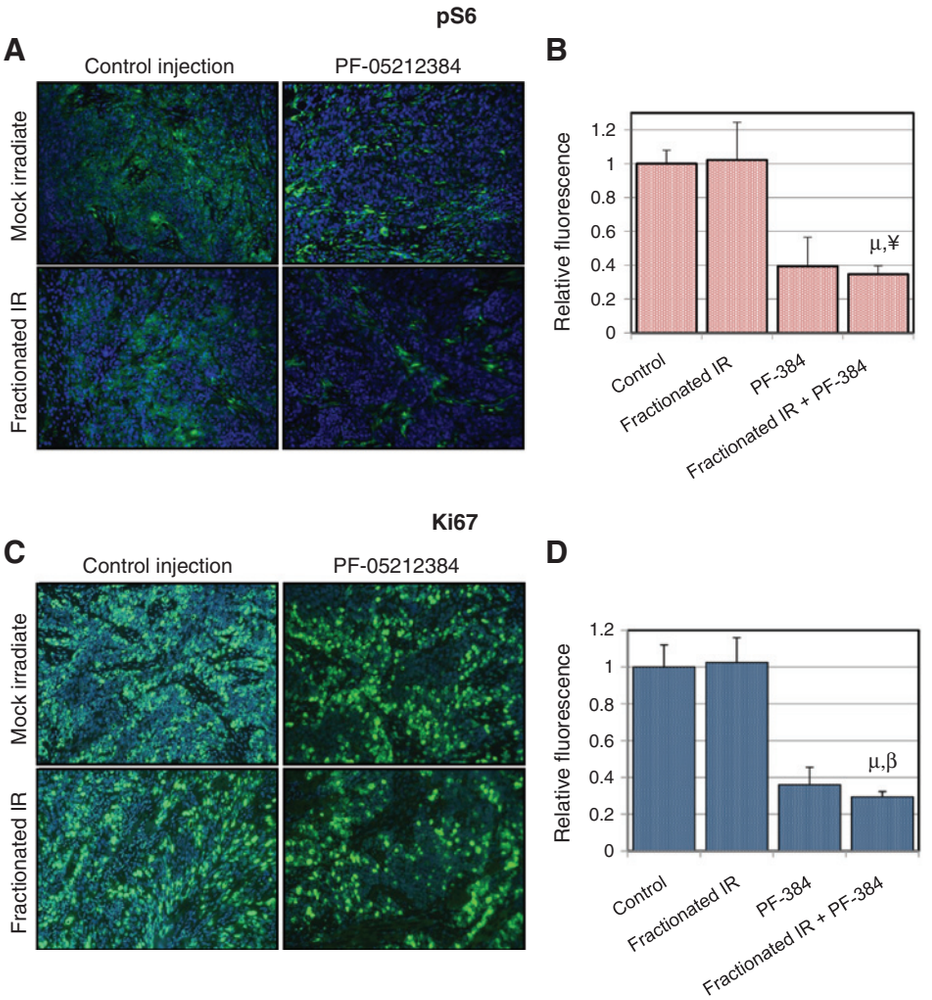

Figure 5.
Representative immunohistochemistry images of UMSCC1 tumor xenograft tissue sections harvested on treatment day 5 (after 5 × 3 Gy fractions and 3 × 6.7 mg/kg PF-05212384 injections). A and B, pS6 (green fluorescence) immunostaining with relative pS6 fluorescence. C and D, Ki67 (green fluorescence) immunostaining with relative Ki67 fluorescence. Relative fluorescence (green fluorescence area/nuclear count) expressed as mean (±SEM) of 3 random fields per mouse for ≥2 mice per treatment group. [¥,β]Fractionated radiation plus PF-05212384 statistically different from fractionated radiation alone ($P < 0.05$ for pS6; $P < 0.0005$ for Ki67). [μ]Fractionated radiation plus PF-05212384 versus PF-05212384 treatment alone not statistically different ($P > 0.05$) for pS6 or Ki67 immunostaining. DAPI nuclear counterstain (blue fluorescence). Statistical analyses performed utilizing Student *t* test. Imaged at ×20 magnification.

genomic expression of fibronectin 1 then may simply represent an attempt to overcome PI3K inhibition. Taken together, it reemphasizes PI3K as a potential radiation modulation target in HNSCC.

PF-05212384 and fractionated IR combination delay UMSCC1 xenograft growth

Based on significant pre- and post-IR PF-05212384 treatment radiosensitization *in vitro*, we next evaluated PF-05212384 with fractionated radiation (3 Gy) *in vivo* via nude mice bearing right flank UMSCC1 xenografts. A preliminary *in vivo* experiment demonstrated that fewer than three PF-05212384 (20 mg/kg/week) injections per week resulted in no radiosensitization. Mice were irradiated (3 Gy fraction) daily from Monday to Friday, with a weekend hiatus, for 2 weeks. During the 2-week fractionated radiation course, PF-05212384 (6.7 mg/kg) was delivered via tail vein injection on Monday, Wednesday, and Friday 2 hours before irradiation. In the absence of radiation, PF-05212384 had a small effect on UMSCC1 xenograft growth with time to thrice initial tumor volume of 3.1 (±0.9) days ($P = 0.04$) versus control (Fig. 4A). Days to thrice initial tumor volume relative to control for fractionated radiation and fractionated radiation + PF-05212384 were 7.1 (±1.4; $P < 0.005$) and 13.0 (±1.6; $P < 5.0 \times 10^{-6}$), respectively. Fractionated radiation + PF-05212384 UMSCC1 xenograft regrowth was significantly prolonged (5.9 days) relative to fractionated radiation alone ($P < 0.05$). Combined treatment (fractionated radiation + PF-05212384) growth delay of 13.0 days demonstrates a synergistic effect as the sum of the individual treatments equates to 10.2 days.

Moderately reduced PI3K/mTOR inhibition with PF-05212384 and fractionated IR in UMSCC1 tumor xenografts

To assess the molecular inhibition of PI3K and mTOR in HNSCC tumor xenografts, we analyzed the downstream targets Akt, S6, and 4EBP1 on day 5 of treatment with immunoblotting, as well as immunohistochemistry of the mTORC1 phosphorylation target S6. The mTORC1 downstream targets 4EBP1 and S6 demonstrated moderately reduced phosphorylation, with no difference in mTORC1 inhibition between xenografts treated with drug alone and xenografts treated with drug plus fractionated radiation (Fig. 4B). Inhibition of the mTORC2 was verified by reduced phosphorylation of the protein kinase Akt. As with S6 and 4EBP1, xenografts treated with drug plus radiation displayed an equivalent level of reduced pAkt as in the xenografts treated with drug alone. In addition to xenograft lysate immunoblotting, immunohistochemistry of xenograft tissue sections demonstrated reduced pS6 (green) fluorescence in drug-treated xenografts, as shown in Fig. 5A and B. Drug-treated irradiated xenografts

displayed a statistically significant ($P< 0.05$) reduction in pS6 fluorescence versus irradiated xenografts with no drug treatment. In addition to downstream target inhibition, cellular proliferation was significantly ($P < 0.0005$) reduced in tumor xenografts treated with drug versus no drug as indicated by Ki67 (green) immunohistochemistry shown in Fig. 5C and D. There was no difference in Ki67 fluorescence between drug treatment alone xenografts and irradiated plus drug treatment xenografts. This is consistent with the cytostatic effect of PF-05212384 and the timeframe of UMSCC1 xenograft radiation regrowth delay (see Fig. 4A).

Discussion

The identification of viable clinical radiosensitizers necessitates extensive preclinical investigation into treatment schedule, efficacy, biomarker identification, and normal tissue toxicity (42). With the identification of the PI3K/mTOR axis as a potential radiation modulation target in HNSCC, we sought to investigate the dual PI3K/mTOR inhibitor PF-05212384 as a radiosensitizer through rigorous preclinical investigation. Through our use of multiple treatment schedules, we have found that dual PI3K/mTOR inhibition significantly radiosensitizes HNSCC tumor cells with PF-05212384 treatment following irradiation, with variable radiation enhancement following a pre-IR treatment regimen (Fig. 1). Regardless of p53 status, dramatic radiosensitization was evident in all HNSCC cell lines studied with PF-05212384 treatment following irradiation. Importantly, radiosensitization occurring in normal fibroblasts was significantly reduced as compared with malignant cells (post-IR treatment DMF of 1.4 vs. $\geq$1.9, respectively). To ascertain efficacy, we show that PF-05212384 (i.v.) with fractionated radiation synergistically delays UMSCC1 xenograft regrowth (Fig. 4A). Along with the key finding of UMSCC1 xenograft regrowth delay, multiple potential clinical pharmacodynamic effects on targets were identified, including pAkt, p4EBP1, pS6, and Ki67 (Figs. 4B and 5). Overall, the significant targeted radiation modulation along with the extensive preclinical investigation presented here supports clinical assessment of PF-05212384 as a radiosensitizer in the combined modality treatment of HNSCC.

An incentive for utilizing a molecular targeted agent in combination with radiation for the treatment of HNSCC is the potential for differentially abrogating tumor cell radiation response versus normal tissue. A number of PI3K, mTOR, and dual PI3K/mTOR inhibitors have been tested in hopes of achieving a differential radiation response. One such agent, the dual PI3K/mTOR inhibitor NVP-BEZ-235, radiosensitizes a number of tumor cell lines (18, 20–22). However, as stated earlier, a major component of this compound's radiosensitization is secondary to off-target effects via catalytic inhibition of the key DNA repair enzymes DNA-PKc and ATM, which could hinder this drug's use in combination with radiation near the rapidly proliferative oral and pharyngeal mucosa. Here, we not only demonstrated PF-052123384 did not alter levels of activated DNA-PKc and ATM enzymes directly (Supplementary Fig. S5), but by clonogenic assay, normal fibroblasts were radiosensitized to a lesser extent as compared with tumor cells (Fig. 1). Notably, inhibition of the PI3K/mTOR pathway has been noted to reduce cellular mitochondrial oxygen consumption preventing tumor hypoxia (43). In a clinical setting, reduced tumor hypoxia could result in an enhanced radiation response, but this mechanism could not account for reduced normal tissue radiation enhancement as compared with HNSCC *in vitro*, particularly the studies performed here, as all cell cultures comparing normal versus tumor cells were performed at constant atmospheric oxygen level on exponentially growing cells (i.e., equivalent free radical formation). Although not directly inhibiting DNA-DSB repair enzymes, targeting the PI3K/mTOR axis with PF-05212384 clearly abrogates DNA-DSB repair following ionizing radiation as evidenced by a statistically significant ($P< 0.05$) delay in phosphorylated γH2AX resolution with PF-05212384 24-hour treatment versus no treatment (Fig. 3). The exact mechanism or mechanisms linking dual PI3K/mTOR inhibition to ionizing radiation–induced DNA-DSB repair inhibition remain to be elucidated.

To further assess PF-05212384 mechanism in conjunction with IR, cellular senescence PCR array analysis was performed. As was expected, dual PI3K/mTOR inhibitor had significant effects on both cell cycle–active and cell cycle inhibition genes (Supplementary Table S1). All the cyclins (A, B, and D) were markedly downregulated, and several cyclin-dependent kinase inhibitors were upregulated (CDKN1A, CDKN1C, p53, and CDKN2B). The net effect on these genes was consistent with the cell cycle flow analysis showing a significant block in G_1 and a loss in S and G_2 phases (Table 1). A potentially interesting finding was that PF-05212384 downregulated several genes involved in DNA damage response (Table 1) and that this might be the mechanism of radiosensitization in the UMSCC1 cells. Additional experiments to determine if these genes are altered in UMSCC46 cells and normal fibroblasts are planned.

As has been reiterated throughout the literature and reinforced by clinical trials, an effective molecular targeted agent spares normal tissue while at the same time synergistically killing tumor cells in conjunction with radiation. An agent's ability to radiosensitize tumor cells *in vitro* is most often assessed by survival of exponentially growing cells following drug plus IR exposure. However, an exponentially growing clonogenic cell population bathed in nutrient-rich growth medium at best represents a fraction of the cellular system near vasculature within a three-dimensional malignant tumor. A large fraction of the tumor, in contrast, lies at a considerable distance from the nearest blood vessel. This tumor microenvironment is distinct from normal physiologic conditions and is characterized by a reduction in proliferative rate, extracellular pH, oxygen tension, and nutrients, with an increase in lactic acid and catabolites (44, 45). To appropriately model this distinct noncycling cellular population, considerable efforts were expounded in the early 1970s, identifying plateau-phase monolayer cultures as a system closely resembling a hypoxic microenvironment (46). Here, we have demonstrated that PF-05212384 via dual PI3K/mTOR inhibition significantly radiosensitizes plateau-phase UMSCC1 tumor cells with pretreatment and posttreatment DMFs of 1.6 and 2.2, respectively (Supplementary Fig. S1B). Radiosensitization of the nonproliferative and proliferative HNSCC cellular populations *in vitro*, in conjunction with the validating synergistic UMSCC1 xenograft regrowth delay *in vivo*, strongly support PF-05212384 as an agent capable of radiosensitization in physiologic and nonphysiologic tumor microenvironments. These results using fractionated radiation, together with preliminary data using single large doses of radiation combined with PF-04691502, indicate that PI3K/mTOR inhibition may be a good target for clinical radiotherapy (17).

Experimental evidence has surfaced indicating PF-05212384 dual PI3K/mTOR inhibition rescues HNSCC from cetuximab resistance (47). The ability to resensitize tumor cells previously

resistant to a known radiosensitizing agent indicates PF-05212384, a significant radiosensitizing agent solely by itself, could potentially be quite efficacious for the treatment of cetuximab-resistant HNSCC. However, PF-05212384 as a rescue therapeutic necessitates the combination of multiple molecular targeted agents in combination with radiation. A phase II clinical trial, RTOG 0411, and a phase III clinical trial, RTOG 0522, have assessed the impact on survival with the addition of molecular targeted agents, bevacizumab and cetuximab, respectively, to concurrent chemoradiation. The addition of a molecular targeted agent in both clinical trials did not improve outcome. Although increased toxicity may have played a role as a consequence of treatment breaks, a criticism of these clinical trials is the lack of biomarker studies and the inability to assess appropriate target inhibition (42). In this study, several tissue proteins were identified from our UMSCC1 xenograft regrowth delay studies, including pAkt, p4EBP1, pS6, and Ki67, that could be evaluated as candidate biomarkers to guide future clinical trials investigating PF-05212384 as a radiosensitizing agent (Figs. 4B and 5). The identification of multiple potential surrogates is key as DNA-damaging agents, such as cisplatin, modulate components of the mTOR signaling pathway (48, 49).

The data presented here represent the most comprehensive preclinical evidence that true dual PI3K/mTOR inhibition by PF-05212384 radiosensitizes HNSCC, with limited normal fibroblast radiation enhancement. Before the initiation of clinical trials investigating PF-05212384 in the combined modality treatment of HNSCC, a few key issues need to be addressed. Immunosuppressant mTOR inhibitors, such as everolimus, have a narrow therapeutic window with high concentrations resulting in serious adverse effects (50). Thus, it will be a necessity to carefully craft the PF-05212384 treatment schedule and dose when combined with radiation based both on extensive preclinical data and current in human phase I to II clinical trials. In addition, although multiple potential biomarkers were identified, the most appropriate biomarker or permutation of biomarkers establishing clinically relevant outcomes remains to be clarified. In the context of cetuximab resistance, PF-05212384 action as a resensitizing agent may prove to be quite efficacious reinforcing appropriate schedule, dosing, and clinical biomarker identification. Finally, this study lays the foundation for further investigation into the PI3K/mTOR axis as a radiation modulation target in HNSCC and has identified the dual PI3K/mTOR inhibitor PF-05212384 as a potential clinical radiosensitizer.

Disclosure of Potential Conflicts of Interest

No potential conflicts of interest were disclosed.

Authors' Contributions

Conception and design: A.J. Leiker, C. Van Waes, J.B. Mitchell
Development of methodology: A.J. Leiker, R. Choudhuri, J.A. Cook, J.B. Mitchell
Acquisition of data (provided animals, acquired and managed patients, provided facilities, etc.): A.J. Leiker, W. DeGraff, R. Choudhuri, A.L. Sowers, A. Thetford
Analysis and interpretation of data (e.g., statistical analysis, biostatistics, computational analysis): A.J. Leiker, J.A. Cook
Writing, review, and/or revision of the manuscript: A.J. Leiker, J.A. Cook, C. Van Waes, J.B. Mitchell
Administrative, technical, or material support (i.e., reporting or organizing data, constructing databases): W. DeGraff, A.L. Sowers, A. Thetford
Study supervision: J.A. Cook, J.B. Mitchell

Acknowledgments

The authors thank Pfizer Oncology for kindly providing PF-05212384.

Grant Support

This research was supported by the Intramural Research Program of the Center of Cancer Research, National Cancer Institute, and National Institute on Deafness and Other Communication Disorders (Project ZIA-DC-000016 and 000073), National Institutes of Health. A.J. Leiker was supported in part by the NIH Medical Research Scholars Program, a public–private partnership supported jointly by the NIH and generous contributions to the Foundation for the NIH from Pfizer Inc., The Doris Duke Charitable Foundation, The Alexandria Real Estate Equities, Inc. and Mr. and Mrs. Joel S. Marcus, and the Howard Hughes Medical Institute, as well as other private donors.

The costs of publication of this article were defrayed in part by the payment of page charges. This article must therefore be hereby marked *advertisement* in accordance with 18 U.S.C. Section 1734 solely to indicate this fact.

Received December 19, 2014; revised February 23, 2015; accepted February 23, 2015; published OnlineFirst February 27, 2015.

References

1. Siegel R, Ma J, Zou Z, Jemal A. Cancer statistics, 2014. CA Cancer J Clin 2014;64:9–29.
2. Baxi SS, Pinheiro LC, Patil SM, Pfister DG, Oeffinger KC, Elkin EB. Causes of death in long-term survivors of head and neck cancer. Cancer 2014;120:1507–13.
3. Bonner JA, Harari PM, Giralt J, Azarnia N, Shin DM, Cohen RB, et al. Radiotherapy plus cetuximab for squamous-cell carcinoma of the head and neck. N Engl J Med 2006;354:567–78.
4. Vermorken JB, Mesia R, Rivera F, Remenar E, Kawecki A, Rottey S, et al. Platinum-based chemotherapy plus cetuximab in head and neck cancer. N Engl J Med 2008;359:1116–27.
5. Kalyankrishna S, Grandis JR. Epidermal growth factor receptor biology in head and neck cancer. J Clin Oncol 2006;24:2666–72.
6. Pfister DG, Ang KK, Brizel DM, Burtness BA, Cmelak AJ, Colevas AD, et al. Head and neck cancers. J Natl Compr Canc Netw 2011;9:596–650.
7. The cancer genome atlas [http://cancergenome.nih.gov/]. [cited March 22nd, 2015].
8. The cancer genome atlas network. Comprehensive genomic characterization of head and neck squamous cell carcinomas. Nature 2015;517:576–82.
9. Broek RV, Mohan S, Eytan DF, Chen Z, Van Waes C. The PI3K/Akt/mTOR axis in head and neck cancer: functions, aberrations, crosstalk, and therapies. Oral Dis 2013 Nov 12. [Epub ahead of print].
10. Freudlsperger C, Burnett JR, Friedman JA, Kannabiran VR, Chen Z, Van Waes C. EGFR-PI3K-AKT-mTOR signaling in head and neck squamous cell carcinomas: attractive targets for molecular-oriented therapy. Expert Opin Ther Targets 2011;15:63–74.
11. Chang L, Graham PH, Hao J, Ni J, Bucci J, Cozzi PJ, et al. Acquisition of epithelial-mesenchymal transition and cancer stem cell phenotypes is associated with activation of the PI3K/Akt/mTOR pathway in prostate cancer radioresistance. Cell Death Dis 2013;4:e875.
12. McKenna WG, Muschel RJ, Gupta AK, Hahn SM, Bernhard EJ. The RAS signal transduction pathway and its role in radiation sensitivity. Oncogene 2003;22:5866–75.
13. Dent P, Yacoub A, Contessa J, Caron R, Amorino G, Valerie K, et al. Stress and radiation-induced activation of multiple intracellular signaling pathways. Radiat Res 2003;159:283–300.
14. Gupta AK, McKenna WG, Weber CN, Feldman MD, Goldsmith JD, Mick R, et al. Local recurrence in head and neck cancer: relationship to

radiation resistance and signal transduction. Clin Cancer Res 2002;8:885–92.
15. Hayman TJ, Wahba A, Rath BH, Bae H, Kramp T, Shankavaram UT, et al. The ATP-competitive mTOR inhibitor INK128 enhances in vitro and in vivo radiosensitivity of pancreatic carcinoma cells. Clin Cancer Res 2014;20:110–9.
16. Gupta AK, Cerniglia GJ, Mick R, Ahmed MS, Bakanauskas VJ, Muschel RJ, et al. Radiation sensitization of human cancer cells in vivo by inhibiting the activity of PI3K using LY294002. Int J Radiat Oncol Biol Phys 2003;56: 846–53.
17. Herzog A, Bian Y, Vander Broek R, Hall B, Coupar J, Cheng H, et al. PI3K/mTOR inhibitor PF-04691502 antitumor activity is enhanced with induction of wild-type TP53 in human xenograft and murine knockout models of head and neck cancer. Clin Cancer Res 2013;19:3808–19.
18. Kim KW, Myers CJ, Jung DK, Lu B. NVP-BEZ-235 enhances radiosensitization via blockade of the PI3K/mTOR pathway in cisplatin-resistant non-small cell lung carcinoma. Genes Cancer 2014;5:293–302.
19. Fokas E, Im JH, Hill S, Yameen S, Stratford M, Beech J, et al. Dual inhibition of the PI3K/mTOR pathway increases tumor radiosensitivity by normalizing tumor vasculature. Cancer Res 2012;72:239–48.
20. Potiron VA, Abderrahmani R, Giang E, Chiavassa S, Di Tomaso E, Maira SM, et al. Radiosensitization of prostate cancer cells by the dual PI3K/mTOR inhibitor BEZ235 under normoxic and hypoxic conditions. Radiother Oncol 2013;106:138–46.
21. Mukherjee B, Tomimatsu N, Amancherla K, Camacho CV, Pichamoorthy N, Burma S. The dual PI3K/mTOR inhibitor NVP-BEZ235 is a potent inhibitor of ATM- and DNA-PKCs-mediated DNA damage responses. Neoplasia 2012;14:34–43.
22. Gil del Alcazar CR, Hardebeck MC, Mukherjee B, Tomimatsu N, Gao X, Yan J, et al. Inhibition of DNA double-strand break repair by the dual PI3K/mTOR inhibitor NVP-BEZ235 as a strategy for radiosensitization of glioblastoma. Clin Cancer Res 2014;20:1235–48.
23. Davis AJ, So S, Chen DJ. Dynamics of the PI3K-like protein kinase members ATM and DNA-PKcs at DNA double strand breaks. Cell Cycle 2010; 9:2529–36.
24. Moding EJ, Kastan MB, Kirsch DG. Strategies for optimizing the response of cancer and normal tissues to radiation. Nat Rev Drug Discov 2013;12: 526–42.
25. Moding EJ, Lee CL, Castle KD, Oh P, Mao L, Zha S, et al. Atm deletion with dual recombinase technology preferentially radiosensitizes tumor endothelium. J Clin Invest 2014;124:3325–38.
26. Ang KK, Zhang Q, Rosenthal DI, Nguyen-Tan PF, Sherman EJ, Weber RS, et al. Randomized phase III trial of concurrent accelerated radiation plus cisplatin with or without cetuximab for stage III to IV head and neck carcinoma: RTOG 0522. J Clin Oncol 2014;32:2940–50.
27. Venkatesan AM, Dehnhardt CM, Delos Santos E, Chen Z, Dos Santos O, Ayral-Kaloustian S, et al. Bis(morpholino-1,3,5-triazine) derivatives: potent adenosine 5′-triphosphate competitive phosphatidylinositol-3-kinase/mammalian target of rapamycin inhibitors: discovery of compound 26 (PKI-587), a highly efficacious dual inhibitor. J Med Chem 2010;53:2636–45.
28. Reiss M, Brash DE, Munoz-Antonia T, Simon JA, Ziegler A, Vellucci VF, et al. Status of the p53 tumor suppressor gene in human squamous carcinoma cell lines. Oncol Res 1992;4:349–57.
29. Albright N. Computer programs for the analysis of cellular survival data. Radiat Res 1987;112:331–40.
30. Mitchell JB, Choudhuri R, Fabre K, Sowers AL, Citrin D, Zabludoff SD, et al. In vitro and in vivo radiation sensitization of human tumor cells by a novel checkpoint kinase inhibitor, AZD7762. Clin Cancer Res 2010;16:2076–84.
31. Soule BP, Simone NL, DeGraff WG, Choudhuri R, Cook JA, Mitchell JB. Loratadine dysregulates cell cycle progression and enhances the effect of radiation in human tumor cell lines. Radiat Oncol 2010;5:8,717X-5–8.
32. Yoshizumi T, Brady SL, Robbins ME, Bourland JD. Specific issues in small animal dosimetry and irradiator calibration. Int J Radiat Biol 2011;87: 1001–10.
33. Alvarez ML, Done SC. SYBR(R) green and TaqMan(R) quantitative PCR arrays: expression profile of genes relevant to a pathway or a disease state. Methods Mol Biol 2014;1182:321–59.
34. Ducker GS, Atreya CE, Simko JP, Hom YK, Matli MR, Benes CH, et al. Incomplete inhibition of phosphorylation of 4E-BP1 as a mechanism of primary resistance to ATP-competitive mTOR inhibitors. Oncogene 2014;33:1590–600.
35. Hayman TJ, Kramp T, Kahn J, Jamal M, Camphausen K, Tofilon PJ. Competitive but not allosteric mTOR kinase inhibition enhances tumor cell radiosensitivity. Transl Oncol 2013;6:355–62.
36. Feng Z, Zhang H, Levine AJ, Jin S. The coordinate regulation of the p53 and mTOR pathways in cells. Proc Natl Acad Sci U S A 2005;102: 8204–9.
37. Ben-Porath I, Weinberg RA. The signals and pathways activating cellular senescence. Int J Biochem Cell Biol 2005;37:961–76.
38. Finkel T, Serrano M, Blasco MA. The common biology of cancer and ageing. Nature 2007;448:767–74.
39. Azad A, Jackson S, Cullinane C, Natoli A, Neilsen PM, Callen DF, et al. Inhibition of DNA-dependent protein kinase induces accelerated senescence in irradiated human cancer cells. Mol Cancer Res 2011;9:1696–707.
40. Gorrini C, Loreni F, Gandin V, Sala LA, Sonenberg N, Marchisio PC, et al. Fibronectin controls cap-dependent translation through beta1 integrin and eukaryotic initiation factors 4 and 2 coordinated pathways. Proc Natl Acad Sci U S A 2005;102:9200–5.
41. Jerhammar F, Ceder R, Garvin S, Grenman R, Grafstrom RC, Roberg K. Fibronectin 1 is a potential biomarker for radioresistance in head and neck squamous cell carcinoma. Cancer Biol Ther 2010;10:1244–51.
42. Morgan MA, Parsels LA, Maybaum J, Lawrence TS. Improving the efficacy of chemoradiation with targeted agents. Cancer Discov 2014;4:280–91.
43. Kelly CJ, Hussien K, Fokas E, Kannan P, Shipley RJ, Ashton TM, et al. Regulation of O2 consumption by the PI3K and mTOR pathways contributes to tumor hypoxia. Radiother Oncol 2014;111:72–80.
44. Horowitz IA, Norwint H, Hall EJ. Conditioned medium from plateau-phase cells. effect on growth of proliferative cells and on repair of potentially lethal radiation damage. Radiology 1975;114:723–6.
45. Phillips RM, Clayton MR. Plateau-phase cultures: an experimental model for identifying drugs which are bioactivated within the microenvironment of solid tumours. Br J Cancer 1997;75:196–201.
46. Hahn GM, Little JB. Plateau-phase cultures of mammalian cells: an in vitro model for human cancer. Curr Top Radiat Res Q 1972;8:39–43.
47. D'Amato V, Rosa R, D'Amato C, Formisano L, Marciano R, Nappi L, et al. The dual PI3K/mTOR inhibitor PKI-587 enhances sensitivity to cetuximab in EGFR-resistant human head and neck cancer models. Br J Cancer 2014;110:2887–95.
48. O'Reilly T, McSheehy PM. Biomarker development for the clinical activity of the mTOR inhibitor everolimus (RAD001): processes, limitations, and further proposals. Transl Oncol 2010;3:65–79.
49. Tee AR, Proud CG. DNA-damaging agents cause inactivation of translational regulators linked to mTOR signalling. Oncogene 2000; 19:3021–31.
50. Moes DJ, Press RR, den Hartigh J, van der Straaten T, de Fijter JW, Guchelaar HJ. Population pharmacokinetics and pharmacogenetics of everolimus in renal transplant patients. Clin Pharmacokinet 2012;51:467–80.